Laser and Particle Beams (2007), *25*, 15–21. Printed in the USA.

DOI: 10.1017/S0263034607070036

Glass fibers for stimulated Brillouin scattering and phase conjugation

STEFAN MEISTER, THOMAS RIESBECK, AND HANS J. EICHLER
TU Berlin, Optisches Institut, Berlin, Germany

(RECEIVED 9 September 2006; ACCEPTED 25 September 2006)

Abstract

Stimulated Brillouin scattering (SBS) and the laser-induced damage threshold (LIDT) in different multimode glass fibers with a core diameter of 200 μm are determined. Antireflective coatings for fiber end-faces with high LIDT are developed, which enhance the SBS reflectivity and reduce unwanted front-face reflections. The morphology of pump- and Stokes-radiation induced damages is investigated using atomic force microscopy.

Keywords: Glass fiber; Laser-induced damage threshold; Stimulated Brillouin scattering

1. INTRODUCTION

For high power laser systems with relatively low repetition rates (Kong *et al*., 2005*a*), liquids are well suitable as phase conjugating mirrors (PCM) due to stimulated Brillouin scattering (SBS). Very stable operation of liquid PCMs for repetition rates of 10 Hz are shown in Kong *et al*. (2005*a*, 2005*b*, 2006). In master oscillator power amplifier (MOPA) systems used for material processing, with average repetition rates of ~2 kHz and up to 150 kHz in each pulse burst, absorption in liquids can lead to fluctuations in the pulse to pulse stability. For such high repetition rates, glass fibers, consisting of fused silica, are well suitable for reliable and stable laser operation (Eichler *et al*., 2002).

The interaction length in fibers is very long because of light guiding and that the fiber core diameter can be selected with respect to the systems pulse energy to obtain the necessary intensity for high reflectivity SBS. The progress in fiber manufacturing forced by the telecommunication industry leads to very pure materials, so the attenuation is negligible for pulsed laser SBS applications. Another important point is that the SBS threshold is nearly independent for the beam quality of the pump beam (Eichler *et al*., 1997). Limitations of optical fibers as PCMs are, on one hand, the fiber core diameter and the numerical aperture, and therefore the maximal beam distortion which can be phase conjugated. On the other hand, the dynamic range of SBS in fibers is limited by the laser-induced damage threshold (LIDT) because of the required strong focusing of the laser beam on the fiber end-face.

It was shown in Eichler *et al*. (1997) that step index multimode glass fibers are well suited as PCMs in MOPA systems. In such systems, a critical point is the careful injection of the pre-amplified beam into the fiber. Very disturbing in MOPA systems is the Fresnel-reflection from the fiber front face. Such ghost pulses become highly amplified because they travel ahead in time compared to the SBS reflected pulse. This can diminish the beam quality and pulse shape of the MOPA output. A tilted fiber front face (for example, 8 degree) avoids the back propagation of the Fresnel-reflected pulse through the amplifier but makes an angle symmetric injection of the beam into the fiber nearly impossible.

We have developed an antireflective (AR) coating for glass fibers with very high LIDT. AR-coatings reduce the Fresnel-losses and so enhance the reflectivity of the PCM, and can strongly reduce ghost pulses in MOPA systems.

In this paper, first we will give some details on the development of AR-coated fibers with high LIDTs. Then, the SBS threshold and reflectivity are measured for different multimode glass fibers. LIDT measurements of the end-faces of these fibers will be shown. The morphology of damages induced by pump- and Stokes-radiation is studied. Based on the results of the measurements, an AR-coated fiber will be selected with a dynamic range comparable to an uncoated fiber.

Address correspondence and reprint requests to: Stefan Meister, TU Berlin, Optisches Institut, P1-1, Strasse des 17. Juni 135, 10623 Berlin, Germany. E-mail: smeister@physik.tu-berlin.de

2. EXPERIMENTAL DETAILS

2.1. Test setup

We used a Q-switched Nd:YAG laser producing 24 ns pulses at 1064 nm as test setup for SBS as well as LIDT measurement. The laser provides maximum pulse energy of 10 mJ. The laser could be operated with a repetition rate of 200 Hz or in a single-shot mode. The near TEM00 beam quality was $M^2 \approx 1.2$.

The complete experimental setup is shown in Figure 1a. Two fast diodes monitor the pulse shapes of the pump as well as the Stokes beam. A half-wave-plate in combination with a Faraday isolator was used as an attenuator. Three joule meters measure the incident, transmitted and reflected pulse energies, respectively. The beam was focused with a single spherical lens to the fiber end-face. The Stokes beam can be measured with a beam analyzing system (Spiricon CCD camera and an 800 mm lens).

Fiber positioning system in the test setup: A CCD camera was used to determine the focal plane of the focused Nd:YAG-laser beam. When the CCD camera is placed in the focal plane, two He–Ne-laser beams are crossed on the CCD chip. One of the He–Ne-laser beams is collinear with the Nd:YAG-laser beam. Then, the CCD camera is removed and a long distance microscope is used to image the overlap of the focused He–Ne-laser beams on the fiber end-face (Fig. 1b). Thereby, the fiber end-face could easily positioned in the focal plane with a accuracy of about $\pm$ 10 μm.

During the LIDT measurements, the long distance microscope was used for online damage detection by observing the scattered He–Ne-laser light from the damaged fiber surface. For the SBS as well as the LIDT measurements, the laser beam was focused with a 40 mm lens to a 35 μm spot on the end-face of the fibers. This injection condition gives the highest transmission with coupling losses of less than 0.5% (Meister *et al.*, 2006).

2.2. Fiber preparation and coating

All tested fibers are cleaved. To achieve mirror like fiber end-faces the tension was adjusted as low as possible so that the fibers were cracked with a short delay. The quality of the cleaved end-faces was investigated by means of optical interference microscopy as well as atomic force microscopy. The rms-roughness of the fiber end-faces was less than 3 nm.

For the AR-coatings, the fiber end-faces were subjected to multi-step cleaning procedures before deposition. Wet chemical as well as high electric field cleaning procedures were tested to achieve AR-coatings with high LIDT. The fiber end-faces were AR-coated with a two-layer-system consisting of Ta_2O_5 and SiO_2. Ta_2O_5 is well suitable as high index material for electron-beam evaporation. With this coating design, the back reflection is strongly suppressed over a broad spectral range. The AR-coatings were deposited by electron-beam evaporation with a deposition rate of 0.5 nm/s.

2.3. Optimization of the AR-coatings

The LIDT of AR-coated fibers are strongly dependent on the fiber preparation and the layer design. Both were optimized by laser-induced damage measurements and the damage morphology was studied by means of atomic force microscopy (AFM) and scanning electron microscopy (SEM). A further problem is also the adhesion of the AR-coating on the fiber end-face. The adhesion of the AR-coating was strongly improved by deposition of an additional buffer layer between the fiber end-face and the Ta_2O_5 layer of the AR-coating. The buffer layer has also a significant influence on the LIDT as shown in Figure 2.

The AR-coating without buffer layer is the weakest coating. The AR-coating was delaminated around the crater within an area of about 100 μm in diameter. So, no residual

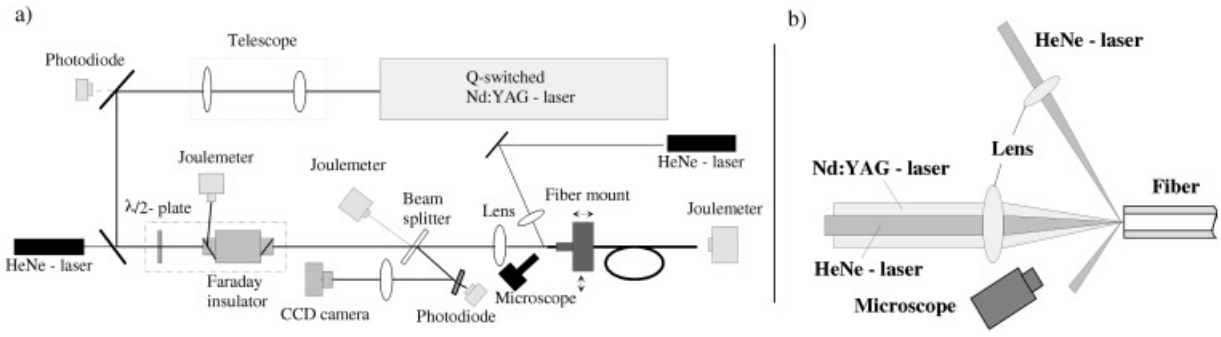

Fig. 1. Scheme of the experimental setup for SBS and LIDT measurement, (**a**) the complete setup and (**b**) online fiber positioning system.

https://doi.org/10.1017/S0263034607070036 Published online by Cambridge University Press

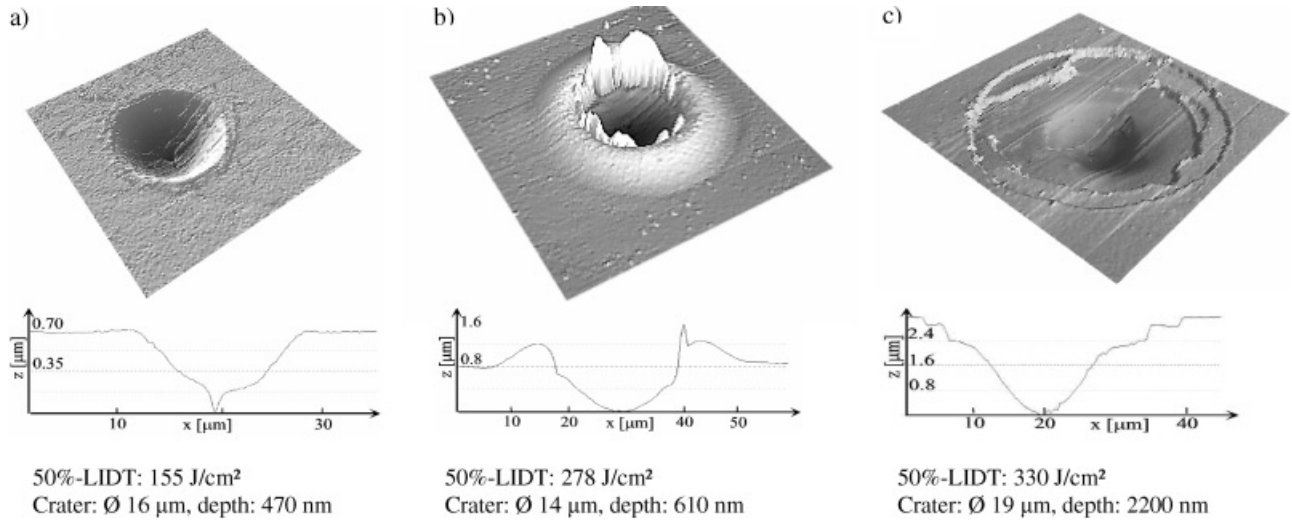

Fig. 2. AFM images of the damaged area induced by a single laser pulse on fiber end-faces with (**a**) an AR-coating without buffer layer, (**b**) an AR-coating with 10 nm buffer layer, and (**c**) an AR-coating with a $\lambda/2$ buffer layer.

AR-coating is seen in the AFM scan (Figure 2a). The crater was burned in the fiber bulk material and had a diameter of 16 μm and a depth of 470 nm.

The AR-coating was improved by a 10 nm buffer layer. The SiO_2 buffer layer has a microscopic amorphous structure and is consisting of the same material as the fiber core. So, the effect of the very thin buffer layer on the reflectivity of the AR-coating should be very low. This AR-coating had a higher LIDT of about 1.8 times. Due to the better adhesion of the AR-coating on the fiber end-face, large area delamination of the AR-coating was prevented (see Figure 2b). The coating is bulged around the ablated area.

The positive effect of the buffer layer on the LIDT can be explained by an improved heat transport due to better adhesion of the coating on the fiber end-face. Also, the structure of the buffer layer is less compact than that of the fiber bulk. Therefore, this layer can buffer some stress induced by differences of the thermal expansion coefficients of the Ta_2O_5 layer compared to the fused silica fiber material.

A further improvement was an AR-coating with a SiO_2 buffer layer with a thickness of $\lambda/2$. The idea was to increase the separation of the weak Ta_2O_5 from the critical fiber bulk-coating interface. Ta_2O_5 has a smaller band gap of about 4.1 eV compared to the $\sim$ 9 eV band gap of SiO_2 (Jasapara *et al.*, 2001). The layer structure of the Ta_2O_5 is polycrystalline and therefore more brittle. The thickness of $\lambda/2$ was chosen to avoid any influence of the buffer layer on the reflectivity of the AR-coating due to discrepancies of the refractive index of the SiO_2 coating compared to the fused silica fiber bulk. The damage morphology in Figure 2c shows a circular ablation of the coating with a diameter of $\sim$40 μm. The single shot 50% LIDT was $H_{50} = 330$ J/cm^2 $\pm$32 J/cm^2. This improved coating design was used for the further investigations.

The optical quality of the AR-coatings was analyzed by means of an optical spectrum analyzer. The residual back reflection of the coating at 1064 nm was -30 dB. It was found that the buffer layers had no measurable influence on the reflectivity of the AR-coatings.

3. RESULTS

3.1. Simulated Brillouin scattering in different 200 μm fibers

The reflectivity of multimode fibers with different core diameters and pure fused silica core is given in Eichler *et al.* (2002). It was found that fibers with 200 μm core diameter are suitable as PCMs in MOPA systems due to a sufficient diameter $\times$ NA product. Here, we will show the results of SBS threshold and reflectivity measurements on four different 200 μm fibers. The parameters of these fibers are listed below.

Tested fibers:

St200	200 μm/220 μm (core/clad) standard step index fiber with a pure fused silica core and very high transparency in the IR region and a numerical aperture of NA = 0.22
GeSI200	200 μm/220 μm step index fiber with a Germanium doped core, NA = 0.4
GeGI200	200 μm/277 μm graded index fiber with a Germanium doped core, NA = 0.28
HPCS200	200 μm/249 μm step index fiber with a pure fused silica core and a hard plastic clad, NA = 0.37

In this measurement, the Gaussian shaped laser pulse was tightly focused to a 35 μm spot on the fiber end-face. The laser was operated in longitudinal single mode with a coherence length of more than 3 m. All tested fibers had a length of 2 m.

In Figure 3, one see big differences in the SBS thresholds for the four different 200 μm fibers. The maximum reflectivities were limited by optical damage under this launching

https://doi.org/10.1017/S0263034607070036 Published online by Cambridge University Press

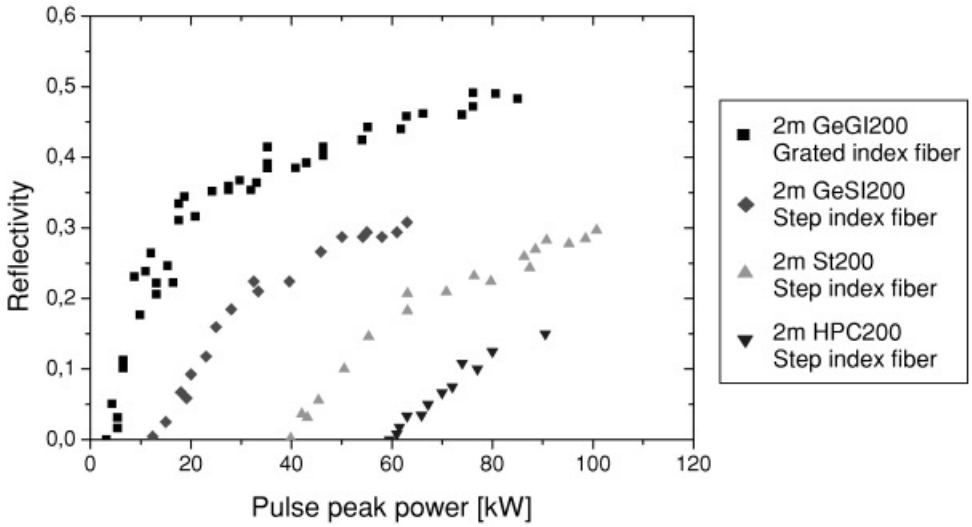

Fig. 3. Internal SBS reflectivity of different multimode fibers with a core diameter of 200 μm.

conditions. The SBS threshold can be estimated with the frequently used equation:

$$P_{th} \approx 21 \cdot \frac{A_{eff}}{L_{eff} \cdot g_B}, \quad (1)$$

where g_B is the Brillouin gain coefficient (Agrawal, 1995). L_{eff} is the length of the reflecting sound wave grating which depends on the coherence length of the laser source. Measurements of the SBS threshold dependent on the fiber length gave a strong increase of the threshold for fibers shorter than 2 m for our system. So, the effective length could assumed to be about 2 m. A_{eff} is the cross-section of the light field propagating in the fiber. The light field distribution and therefore A_{eff} can not be estimated in an easy way. CCD images of the light transmitted through the fibers are shown in Figure 4. For all fibers, exept the HPC fiber, the transmitted light field has a nearly Gaussian shape, which indicates that the light is only guided in the lower fiber modes (Fig. 4a).

The transmitted light through the HPC200 fiber shows a nearly flat top shape (Fig. 4b). The reason could be strong mode mixing forced by an optical inhomogenius polymer material in the cladding. So, this fiber seems to be suitable for high power pulse transmission, if SBS is unwanted.

If we assume A_{eff} to be equal to the fiber cross-section for the HPC200 fiber (ignore that effective mode mixing needs a finite traveling distance) and with $g_B = 2.5$ cm/GW yields a threshold of: $P_{thT} = 13$ kW. The measured 1%-threshold is $P_{thM} = 61$ kW and so about 5 times higher than the calculated threshold. For the other fibers, the effective diameter is much smaller leading to even smaller calculated SBS thresholds.

The standard St200 fiber with pure fused silica core shows a SBS threshold of 41 kW. The GeSI200 fiber with the Germanium doped core shows at $P_{th} = 14$ kW, a significant lower SBS threshold than the St200 fiber. Both fibers are step index fibers. The GeSI200 fiber has a higher NA than the St200 fiber. But the mode field radius should only

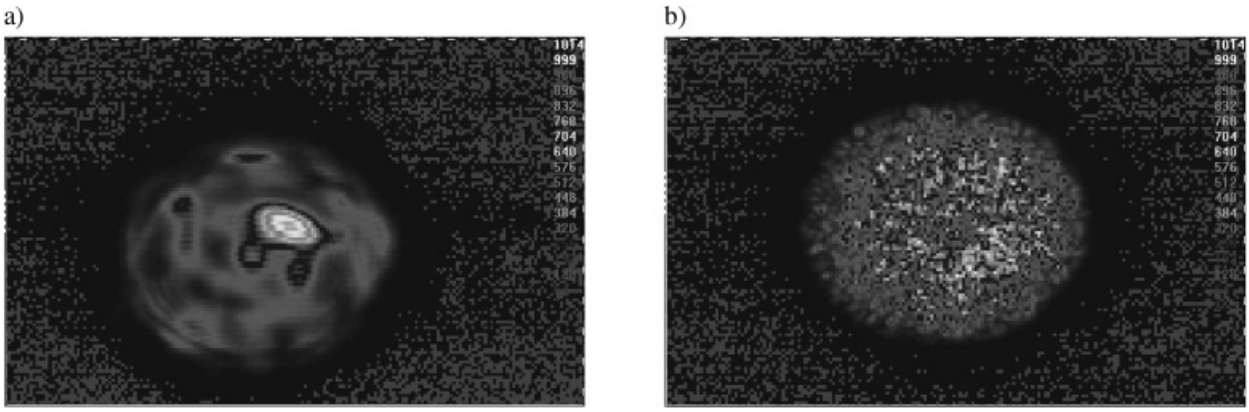

Fig. 4. Transmitted light field at the exit of the fibers. (**a**) St200 fiber and (**b**) HPC200 fiber.

https://doi.org/10.1017/S0263034607070036 Published online by Cambridge University Press

be sligthly smaller if the launching conditions are the same. So, the lower SBS-threshold of the GeSI200 should be related to an higher gain coefficient of the fiber material.

The grated index GeGI200 fiber shows the lowest threshold of $P_{th} = 5$ kW. It is known that grated index fibers are not suited for phase conjugation, because the higher spatial frequencies of the focused pump beam receive lower SBS gain. In Lombard *et al.* (2006), this feature is explained by a higher overlap of the lower fiber modes. The authors suggests a setup containing a long grated index fiber. Here, the SBS in the grated index fiber is used for effective beam cleaning. The higher mode overlap explains the lower SBS threshold of the GeGI200 fiber compared to the GeSI200 fiber. But according to our experiments, the higher Germanium doping level in center of the core compared to the outer core region, leading to a gain gradient transverse to the fiber axis, should play an important rule.

Both the St200 fiber and the GeSI200 fiber are well suited as PCMs for different power intervals. The phase distortion of the injected beam can be higher for the GeSI200 fiber because of its higher NA.

3.2. Laser-induced damage measurements of AR-coated and uncoated fibers

In the following section, the results of multishot LIDT measurements of the four different 200 μm fibers are shown. To determine the influence of the AR-coatings on the SBS dynamic range, the LIDTs of the AR-coated fibers are compared to the LIDTs of the uncoated fibers.

We performed an N-on-1 test procedure for the damage measurements. During this procedure, the fiber front-face is irradiated with (for example, 1000) laser pulses at low fluence. This procedure is repeated with higher fluences until laser-induced damage occurs (Kaiser & Pulker, 2003). The results of the multishot LIDT measurements are given in Figure 5.

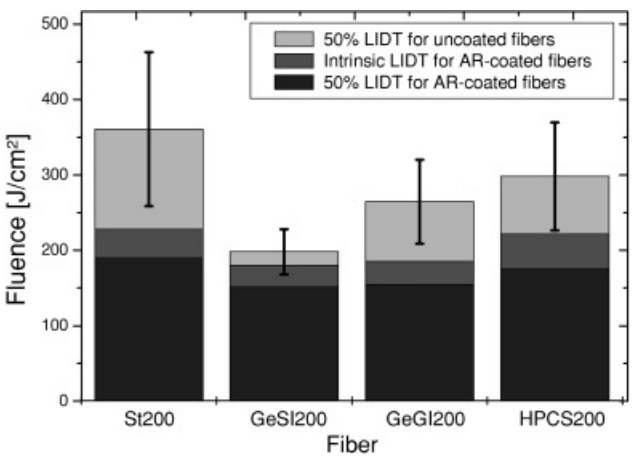

Fig. 5. Multishot laser-induced damage threshold of AR-coated and uncoated 200 μm fibers.

The height of the whole columns corresponds to 50% LIDT of the uncoated fibers with its standard deviation. For the AR-coated fibers, the 50% LIDT is shown as well as the fluence for the occurrence of intrinsic damage. It was found that in multishot tests, the AR-coatings could only withstand a certain maximum amount of fluence which is related to the coating design. If the coatings are damaged at a lower fluence, it can be attributed to the presence of defects.

The uncoated St200 fibers have the highest LIDT followed by the HPCS200 fibers. Both fibers have a pure fused silica core with low OH content. The Germanium doped fibers have a significant lower LIDT. The GeSI200 fibers have the highest dopant concentration. So, one derives a dependence of the LIDT on the Germanium concentration.

The AR-coated St200 fibers had the highest 50% LIDT of 190 J/cm^2 and they break surely at an fluence of 225 J/cm^2. The certain damage fluence as well as the 50% LIDT were for the both Germanium doped fibers, nearly the same but about 15% lower as for the pure fused silica core fibers. While the LIDTs for the uncoated fibers show a strong dependence on the type of fiber, this dependence is much lower for the AR-coated fibers. As a result, the 50% LIDT of the AR-coated GeSI200 fibers reach nearly the same value as for the uncoated GeSI200 fibers.

3.3. Damage morphology of AR-coated fibers under pump- and Stokes-radiation

While in the previous damage measurements, the laser was operated in longitudinal multimode to prevent SBS in the fibers, now it will be shown, damage morphologies of fiber end-faces under pump- and Stokes-radiation imaged by an AFM. Figure 6 shows the damaged area of a St200 fiber and a GeGI200 fiber. The AR-coated fibers were 2 m long. In both cases, the focused laser spot was placed about 40 μm out of fiber axis, to investigate the Stokes compared to the pump beam path.

The St200 fiber was radiated with a fluence of 240 J/cm^2. The Stokes fluence could reach 63 J/cm^2 under this conditions. But it can be expected that a large amount of pump energy was consumed for the damage or reflected on the created plasma. The main crater of the St200 fiber is comparable to the craters in Figure 2 and has a diameter of 21 μm. Inside of this crater a smaller crater with 9 μm in diameter is seen. This crater is created by the Stokes pulse and is located nearly in the center of the main crater. That indicates that the Stokes beam travels the same way as the pump beam even for off-center illumination of the step index wave guide.

The pump- and Stokes-induced craters on the front-face of the grated index GeGI200 fiber are not concentric (Fig. 6b). The smaller Stokes induced crater was located closer to the fiber axis. That indicates that the Stokes beam do not travel the same way as the pump beam. That could be explained by the higher gain in the center of the fiber core, which perfers the lower fiber modes.

https://doi.org/10.1017/S0263034607070036 Published online by Cambridge University Press

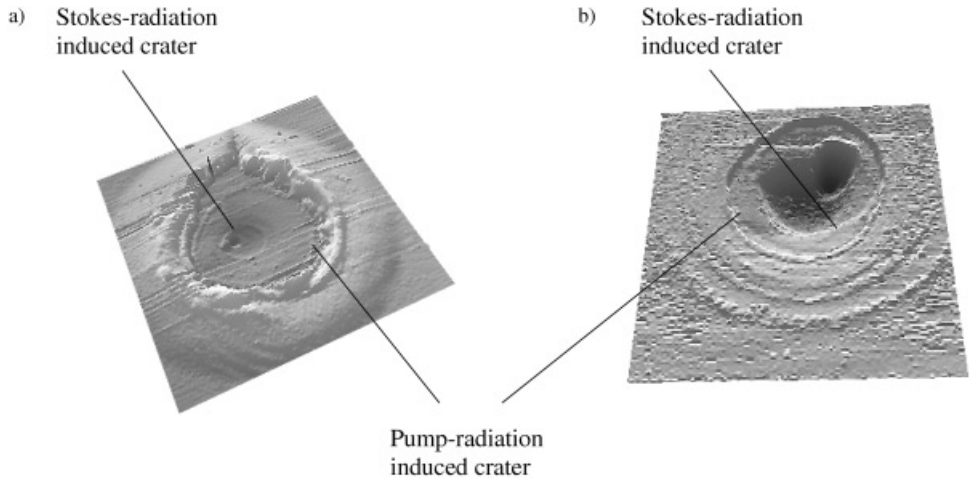

Fig. 6. Damaged area of (**a**) a St200 fiber and (**b**) a GeGI200 fiber.

3.4. Comparison of SBS reflectivity of AR-coated and uncoated fibers

As shown in Section 3.2, the LIDT of uncoated and AR-coated Gemanium doped step index fibers (GeSI200) is nearly in the same range. Therefore, the AR-coatings on the end-face of this fibers have only a small influence on the maximum power, which can be injected into the fiber. The SBS reflectivity of the AR-coated and the uncoated GeSI200 fibers are shown in Figure 7. The maximum reflectivity is in the same range for AR-coated and uncoated fibers, while in the AR-coated fibers, the same reflectivity values are reached at lower pump power. The SBS-reflectivity did not reach saturation before damage because of the tightly focussed beam on the fiber end-face.

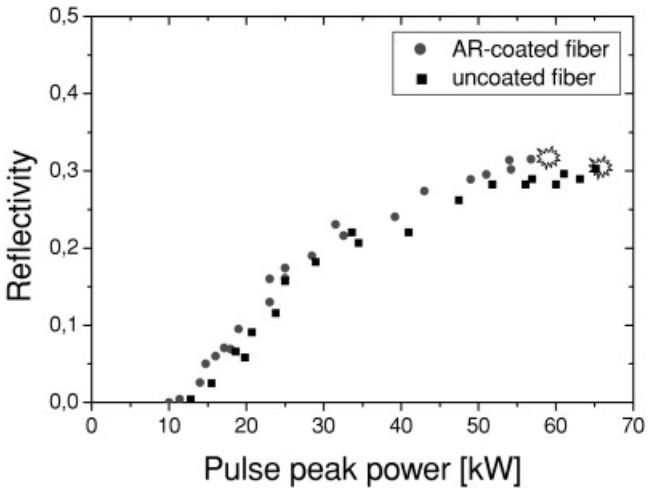

Fig. 7. SBS reflectivity of AR-coated and uncoated Germanium doped 200 mm step index fibers.

4. SUMMARY

The SBS threshold and reflectivity of four different fibers with a core diameter of 200 μm are measured. Step index silica/silica fibers with pure and Germanium doped core are determined as well suited as phase conjugating mirrors. The multishot LIDT measurements on AR-coated and uncoated fibers show that AR-coatings on the Germanium doped fibers do not decrease the SBS dynamic range significantly. By deceasing Fresnel-reflection, the AR-coatings can enhance the performance of fibers as PCMs in MOPA systems.

REFERENCES

Agrawal, G.P. (1995). *Nonlinear fiber optics*. San Diego: Academic Press.

Eichler, H.J., Kunde, J. & Liu, B. (1997). Quartz fiber phase conjugators with high fidelity and reflectivity. *Opt. Comm.* **139**, 327.

Eichler, H.J., Mocofanescu, A., Riesbeck, Th., Risse, E. & Bedau, D. (2002). Stimulated Brillouin scattering in multimode fibers for optical phase conjugation. *Opt. Comm.* **208**, 427–431.

Jasapara, J., Nampoothiri, A.V., Rudolph, W., Ristau, D. & Starke, K. (2001). Femtosecond laser pulse breakdown in dielectric thin films. *Phys. Rev. B* **63**, 045117.

Kaiser, N. & Pulker, H.K. (2003). *Optical Interference Coatings*. Heidelberg: Springer-Verlag.

Kong, H.J., Lee, S.K. & Lee, D.W. (2005*a*). Beam combined laser fusion driver with high power and high repetition rate using stimulated Brillouin scattering phase conjugation mirrors and self-phase-locking. *Laser Part. Beams* **23**, 55–59.

Kong, H.J., Lee, S.K. & Lee, D.W. (2005*b*). Highly repetitive high energy/power beam combination laser: IFE laser driver using independent phase control of stimulated Brillouin scattering phase conjugate mirrors and pre-pulse technique. *Laser Part. Beams* **23**, 107–111.

https://doi.org/10.1017/S0263034607070036 Published online by Cambridge University Press

Kong, H.J., Lee, S.K. & Lee, D.W. (2006). Long term stabilization of the beam combination laser with a phase controlled stimulated Brillouin scattering phase conjugation mirrors for the laser fusion driver. *Laser Part. Beams* **24**, 519.

Lombard, L., Brignon, A., Huignard, J.-P., Lallier, E. & Georges, P. (2006). Beam cleanup in a self-aligned gradient-index Brillouin cavity for high-power multimode fiber amplifiers. *Optics Letters* **31**, 158–160.

Meister, S., Theiss, C., Scharfenorth, C. & Eichler H.J. (2006). Power Transmission Limits of Different Glass Fibers with Antireflective Coating. *Reliability of Optical Fiber Components, Devices, Systems, and Networks III, Proc. SPIE* **6193**, 215–225.

https://doi.org/10.1017/S0263034607070036 Published online by Cambridge University Press